ISSN 2070-0482, Mathematical Models and Computer Simulations, 2009, Vol. 1, No. 6, pp. 724–738. © Pleiades Publishing, Ltd., 2009.
Original Russian Text © A.I. Lebo, I.G. Lebo, 2009, published in Matematicheskoe Modelirovanie, 2009, Vol. 21, No. 1, pp. 75–91.

Interaction of High-Power Laser Pulses with Low-Density Targets in Experiments with the PALS Installation

A. I. Lebo[a] and I. G. Lebo[b]

[a] *Moscow State University, Leninskie gory, Moscow, 119991 Russia*

[b] *Moscow Institute of Radio Engineering and Automation, pr. Vernadskogo 78, Moscow, 119454 Russia*

e-mail: lebo@mirea.ru

Received February 29, 2008

Abstract—Numerical modeling of experiments on the interaction of high-power pulses with low-density porous media is considered. The experimental data were obtained by means of the PALS iodine laser (pulse energy up to 200 J and pulse duration of 0.4 ns). The original density of the porous medium varied from 2.25 to 18 μg/cm^3. A new physico-mathematical model of such plasma is proposed, two-dimensional computations are performed, and good agreement between the calculated and experimental data is shown

DOI: 10.1134/S2070048209060076

1. INTRODUCTION

In nuclear fusion research, multilayer spherical targets are irradiated by a large number of laser beams in order to provide a high irradiation intensity (10^{14}–10^{15} W/cm^2) and uniform heating of the surface. It is impossible to attain a perfectly uniform heating because of the beam overlap, interference in highly coherent beams, nonuniform amplification in the laser channel, defects in amplification channels, and, as a result, formation of a speckled structure of the light front. These perturbations lead to inhomogeneity of the pressure on the evaporation (ablation) surface and to the development of hydrodynamic instability in the process of target implosion. Two methods for flattening the irregularities are discussed in the literature: (1) the use of a symmetrizing prepulse producing a high-temperature plasma crown before the arrival of the main laser pulse [1–4] and (2) the use of a low-density polymer medium [1, 5–8].

In a number of laboratories in different countries, the interaction of laser radiation with porous media [9–19] has been studied.

As a rule, theoretical description of the transfer processes in such structured media is based on conceptions of energy transfer in a weakly inhomogeneous nonturbulent plasma [20–23]. In these works, the numerical modeling of the interaction of laser radiation with such media presumed that the time of the homogenization of structured matter is comparably small and may be neglected. However, to this day, the question whether this assumption is justified remains open. Modeling of energy transfer in subcritical plasma with an allowance for the strong inhomogeneity of the medium (for example, the model of thin films [24] with the structure resembling porous polystirol, which fails to describe a three-dimensional polymer network) is a laborious and difficult problem, requiring additional justification.

The aim of this work is to develop a simplified physico-mathematical model for describing the dynamics of plasma originating from interaction of intensive laser radiation with a low-density medium and compare the calculated and experimental results. This work is based mainly on the results obtained via the PALS installation in Prague [25, 26].

2. BRIEF DESCRIPTION OF THE ATLANT PROGRAM

The numerical experiments were performed using the Atlant program: a two-dimensional Lagrange program in cylindrical geometry (coordinates r, z, t). The two-dimensional equations of gas dynamics and nonlinear heat conduction were solved by the methods developed under the auspices of A.A. Samarskii in the Keldysh Institute of Applied Mathematics and, later, in the Institute for Mathematical Modeling,

Russian Academy of Sciences. Here are the basic equations, which are solved by the finite-difference methods:

$$\frac{d\rho}{dt} = -\rho\nabla\mathbf{V},$$

$$\rho\frac{d\mathbf{v}}{dt} = -\nabla(Z_iP_E + P_I + P_R),$$

$$Z_i\rho\frac{dE_E}{dt} = -Z_iP_E\nabla\mathbf{V} + \nabla(\kappa_E\nabla T_E) - Q_{EI} - Q_{ER} - R_{RAD}(\rho, T_E) + \nabla\mathbf{q},$$

$$\rho\frac{dE_I}{dt} = -P_I\nabla\mathbf{V} + \nabla(\kappa_I\nabla T_I) + Q_{EI},$$

$$\rho\frac{dE_R}{dt} = -P_R\nabla\mathbf{V} + \nabla(\kappa_R\nabla T_R) + Q_{ER}, \tag{1}$$

$$(\mathbf{q}/|\mathbf{q}|, \nabla)\mathbf{q} = k_{ab}(\rho, T_E)\cdot\mathbf{q}, \quad Q_{EI} = c_\nu Z_i\rho\nu_{ei}(T_E - T_I),$$

$$P_E = P_E(\rho, T_E); \quad P_I = P_I(\rho, T_I); \quad P_R = P_R(\rho, T_R),$$

$$E_E = E_E(\rho, T_E); \quad E_I = E_I(\rho, T_I); \quad E_R = E_R(\rho, T_R).$$

Here, ρ is the density; $\mathbf{V}$ is the velocity vector; ν_{ei} is the frequency of the energy exchange between electron and ion components; c_ν is the ion heat capacity; E_E, E_I, and E_R are the specific internal energies of electrons, ions, and photons; E_E and P_E are taken per unit average charge Z_i in a Lagrange cell, R_{RAD} is the energy loss due to reradiation from plasma; and P_E, P_I, P_R, T_E, T_I, and T_R are the electron, ion, and radiation components of the pressure and temperature. According to [27], $\nu_{ei} \sim \frac{m_e}{m_i}\nu_e$ and $Q_{EI} \sim \frac{T_E - T_I}{T_E^{3/2}}Z_i\rho^2$ is the term responsible for the rate of energy exchange between electrons and ions; ν_c is the electron collision frequency; $Q_{ER} = Q_{0ER}\frac{T_E - T_R}{\sqrt{T_E}}Z_i\rho^2$ is the rate of energy exchange between electrons and photons; $\mathbf{q}$ is the laser radiation flux; κ_E, κ_I, and κ_R are the electron, ion, and radiation heat conductances; and k_{ab} is the absorption coefficient. The physico-mathematical model and methods for solving the equation written above are described in more detail in monograph [28].

One can choose between three models for the equation of state of matter: (1) an ideal gas without regard for the ionization and recombination kinetics (the nuclear charge is assumed to be constant in each Lagrange cell); (2) the ZRI model (the Zel'dovich–Raizer model with allowance for ionization). The main ideas of this model were taken from monograph [29] and developed for the calculation of laser plasma in the Department of Quantum Radio Physics of the P.N. Lebedev Physical Institute, the Russian Academy of Sciences [28, 30]. In addition to the equation of state of an ideal two-component plasma (ions and electrons), the ion component involves elastic terms and the electron component takes into account the Fermi degeneration. In each Lagrange cell, the equation of ionization and recombination kinetics are solved in the approximation of the average ion charge; (3) the QEOS (quotidian equations of state) model [31], in which the thermodynamic parameters are specified as tabulated values.

These models are arranged in the order of increasing expenditures of processor time required for solving particular problems.

Generally speaking, the Atlant program takes into account the energy transfer due to reradiation. Moreover, it is assumed that the radiation spectrum corresponds to the Planck spectrum, but with another temperature T_R.[1] Since, in the problems under consideration, the matter has a low ion charge, the contribution of the radiation component to the energy balance is comparatively small. In the calculations presented below, the energy transfer due to reradiation was not taken into account (i.e., a two-temperature

[1] On the basis of the Atlant program, the two-dimensional Latrant program for calculating the radiation problems of gas dynamics in the Lagrange cylindrical coordinates with allowance for radiation transfer in the multigroup approximation has been developed [32].

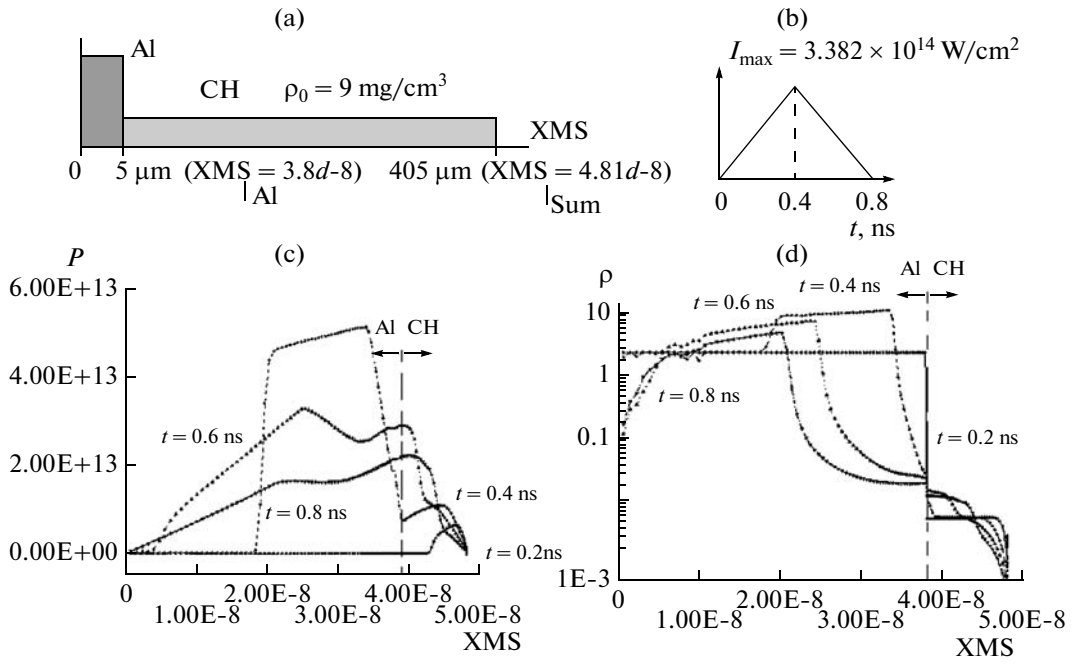

Fig. 1. Schematic view of (a) target and (b) pulse. (a) Positions of boundaries of subdomains expressed in μm and mass coordinates (in brackets). The initial density of external layer is $\rho_0 = 9$ mg/cm^3. (c) Pressure (P) and (d) density (ρ) distributions along the 0Z axis at time points $t = 0.2$, 0.4, 0.6, and 0.8 ns. Laser beam propagates from right to left. The vertical dashed line is the aluminum–polymer interface.

model was used). The first variant of the equations of state of matter has been chosen, i.e., the one corresponding to an ideal gas with a fixed ion charge Z_i.

In the basic Atlant program, it is assumed that the laser radiation propagates along the 0Z axis and is absorbed due to the inverse braking effect. The part of radiation that reaches the critical surface (where the laser radiation frequency becomes equal to the eigenfrequency, from which the critical density $\rho_{cr} = 1.88 \times 10^{-3} \dfrac{A}{Z_i \lambda^2\,[\mu m]}$ [g/cm^3] is found; A is the atomic mass, and λ is the wavelength of the laser radiation expressed in μm) is absorbed in the first Lagrange cell.[2] The absorption coefficient has the form

$$k_{ab}(\rho, T_E) = \left(\frac{\nu_e}{c}\right) \frac{(\omega_p/\omega_0)^2}{\sqrt{1-(\omega_p/\omega_0)^2}} \sim \frac{\rho(\rho/\rho_{cr})}{T_E^{1.5}\sqrt{1-(\rho/\rho_{cr})}}, \quad (2)$$

where ω_p and ω_0 are the plasma and laser frequencies and c is the velocity of light. In the beginning of the process, the radiation is absorbed by the external layers (because, even in a medium with a density below the critical one, the initial temperature is very small); then, along with heating and dispersion of matter, it penetrates to the depth of the target.

3. RESULTS OF NUMERICAL COMPUTATIONS

As follows from the data of the experiments carried out in the PALS installation, when a low-density porous target is irradiated by a laser pulse, a hydrothermal wave propagates in its medium with a velocity of 270 ± 50 km/s (the initial density of the medium being $\rho_0 = 9.1$ mg/cm^3) and 420 ± 70 km/s (the initial density of the medium being $\rho_0 = 4.5$ mg/cm^3) [25].

In the first series of computations, wave propagation in an ordinary medium, with the parameters close to the averaged parameters of foam, was simulated. Figure 1a gives a schematic view of a target containing

[2] In a different version of the Atlant applied program package, models describing the refraction and reflection of laser radiation in cylindrical and spherical geometries were developed (for details, see [33, 34]).

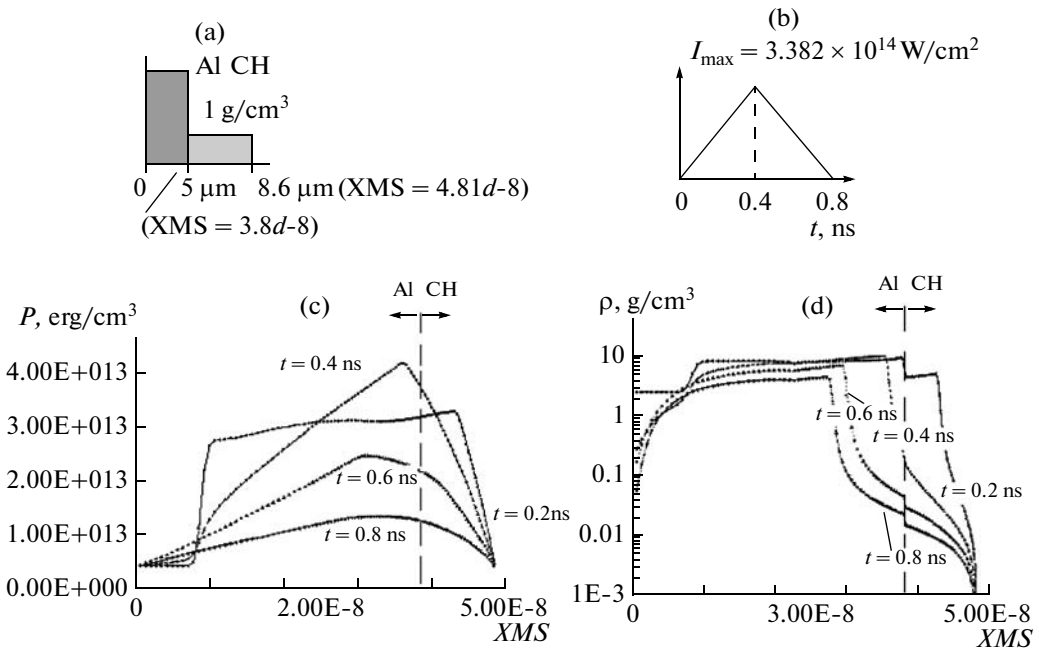

Fig. 2. (a), (b) Setting of the problem and distributions of (c) pressure and (d) density along the 0*Z* axis at the corresponding time instants.

a 400 μm layer of foam with the initial density $\rho_0 = 9$ mg/cm^3 on an aluminum substrate with a thickness of 5 μm. A laser pulse had a temporal form of an isosceles triangle with the time points $t_1 = 0$, $t_2 = 0.4$ ns, and $t_3 = 0.8$ ns as the vertices. The intensity of radiation at the time point $t_2 = 0.4$ ns was I_{max} and varied in different variants of computations from 3×10^{14} to 6×10^{14} W/cm^2.

Such variation of intensity was due to the assumption that a part of laser energy can be reflected and, hence, makes no contribution to the formation of the hydrothermal wave. In the experiment, the laser pulse energy arriving at the target chamber was 170 J, which corresponds to the maximum intensity $I_{max} = 6 \times 10^{14}$ W/cm^2. The fraction of energy reflected from the target was not measured. It should be noted that in the earlier series of experiments on irradiation of aluminum foils that were performed in the PALS installation, the energy loss was approximately 30% [35].

As in the experiments, the laser radiation had a wavelength $\lambda = 0.438$ μm (i.e., the third harmonic of the iodine laser). The computations were carried out in a quasi-one-dimensional setting: a 3×110 computational grid was used, i.e., there were only two Lagrange cells in the 0*R* direction and 109 cells along the 0*Z* axis. In the transverse direction to the 0*Z* axis, the intensity was constant (in this case, 40 cells fell on the foam). Figure 1 represents (a), (b) the setting of the problem and distributions of (c) pressure and (d) density at the time points 0.2, 0.4, 0.6, and 0.8 ns for the case of $I_{max} = 3.38 \times 10^{14}$ W/cm^2.

In the case under consideration, it is more convenient to represent the results of computations in the *XMS* coordinates, i.e., $XMS = \sum_{i=2}^{n} \Delta M_{2j}$, where ΔM_{ij} are the masses of Lagrange cells ($i = 2$ corresponds to a cell adjacent to the 0*Z* axis) and *n* is the number of cells corresponding to a *XMS* coordinate (the aluminum–low-density-matter interface is situated at the point $XMS_b = 3.8 \times 10^{-8}$ a.u.). Below, the distributions of (Fig. 1c) pressure and (Fig. 1d) density at different points of time, obtained in calculations (variant 1) are represented. It is readily seen that, by the time $t_2 = 0.4$ ns, the foam has been heated through and has become transparent. The laser radiation is absorbed in the external aluminum layer and forms a shock wave, which propagates over the aluminum. At the time point 0.6 ns, a discharging wave moves from the back side of the Al foil (the left edge of the target) against the laser beam. At the time point 0.8 ns, dense aluminum layers fly mainly along the laser beam ($XMS_b \le 2.0 \times 10^{-8}$ a.u.) and the remaining plasma, against the laser beam. As follows from [13], the electron heat conductivity in porous media is strongly suppressed. In the second variant, the electronic thermal conductivity coefficient was reduced by a factor of 1000 from the Spitzer one, but, even in this case, the radiation passed the low-density layer by the time $t_2 = 0.4$ ns and, then, after being absorbed in aluminum, formed a shock wave.

The reason of fast wave propagation in low-density matter is that this medium has small mass and low heat capacity. It is instantly heated up, which leads to a fast decrease in the absorption coefficient and the plasma becomes transparent for laser radiation (see (2)).

Figure 2 gives the setting of the problem and results of computations (variant 3) in the case when the target was an aluminum substrate with an applied layer of solid polymer with the initial density $\rho_0 =$ 1 g/cm^3. The mass of the substance in variants 1, 2, and 3 was the same.

In this case, by the time $t_2 = 0.4$ ns, the shock wave has passed through the target and discharging of the material from the back side of the target begins.

Earlier, N.N. Demchenko (Lebedev Physical Institute, RAS) suggested a one-dimensional model of a structured medium in the form of thin polymer layers with a density of 1 g/cm^3, with the gaps between them filled with gas, and propagation of a hydrothermal wave in such a medium was calculated by the RAPID program [36]. The random-access memory of modern personal computers enables one to calculate several tens of such layers. In real situations, the number of layers will be by several orders greater and they will be arranged, generally speaking, at different angles to the wave vector of the laser radiation. Therefore, direct numerical simulation of wave propagation in a structured medium without simplifications is difficult even for modern supercomputers.

Due to the limited capacity of personal computers, the number of layers that can be formed in the two-dimensional setting is several times smaller that in a one-dimensional program. In the following variant, we used a model with three dense layers: the last layer is aluminum and the other two ones are polymer. The gaps between the layers were filled with a gas with an initial density of 2 mg/cm^3. The masses of the layers and of the gas were chosen so that the total bulk weight coincided with the mass in variants 1–3. In addition, the electron and ion thermal conductivities were suppressed in the matter from which the low-density medium (a CH polymer) was produced. Figures 3a and 3b represent the setting of the problem.

Figures 3c and 3d show the density and temperature distributions along the $0Z$ axis at different time instants ($t = 0.2$, 0.4, 0.6, and 0.8 ns).

Figure 3e shows the pressure distribution at different time points. By the time 0.4 ns, the wave passes the CH layer and forms a shock wave in the aluminum substrate. Approximately for 0.1 ns, the shock wave passes aluminum and emerges on the back surface. The layers of matter forming the back surface scatter in the direction of incidence of the laser beam and a discharging wave propagates in compressed aluminum against the laser.

In addition to one-dimensional computations, two-dimensional computations simulating passage of such a wave through a structured target were performed.

The computational grid had dimensions 22×112, and the laser flux had the form $q(t, r) = q_1(t)q_2(r)$. The intensity distribution in the transverse direction had a Gaussian form, i.e., $q_2(t) = \exp[-(r/R_f)^2]$, where $R_f = 150$ μm, and the total energy in a laser pulse was $E_L = 170$ J. Figure 4 shows two-dimensional (a) temperature and (b) density fields at the time point 0.6 ns. The hydrothermal wave reached the interface with aluminum by the time of 0.6 ns, i.e., somewhat later than in previous variants (1–3). Nevertheless, even in this case, the velocity of the wave was about 2–2.5 times grater than in the experiments.

In addition to the results represented above, computations for homogeneous low-density layers were performed for various values of laser intensity and thickness of foam (variants 7–14). In all cases, in order to attain an agreement with the observed propagation of the hydrothermal wave, it was necessary to assume that the absorbed energy is by an order of magnitude smaller than the incident one. Evidently, this assumption did not agree with the conditions of the experiments.

In the subsequent computations, we changed the physical model of absorption of radiation and electron heat transfer. The fraction of laser energy is absorbed at a distance of several wavelengths ($l_p \sim 1$ μm) until this region is homogenized, warmed up, and substantially expanded. Then, the turn of absorption, heating, and scattering of the next portion of matter comes. We considered the following model: the absorption coefficient is determined by the formula

$$k(\rho) = \rho(r, z, t)/(\rho_{cr} l_p), \tag{3}$$

where l_a must be specified a priori.

The absorption of radiation is determined by the law $q_L = q_L^0/\exp(\int_0^z k(\rho)dz)$. The electronic thermal conductivity was reduced by a factor 10^3 from the Spitzer value. The pressure and internal energy vary according to the equation of state of an ideal gas. Along with heating, the pressure increases and the substance is scattered; then, subsequent portions of laser energy penetrate into deeper layers.

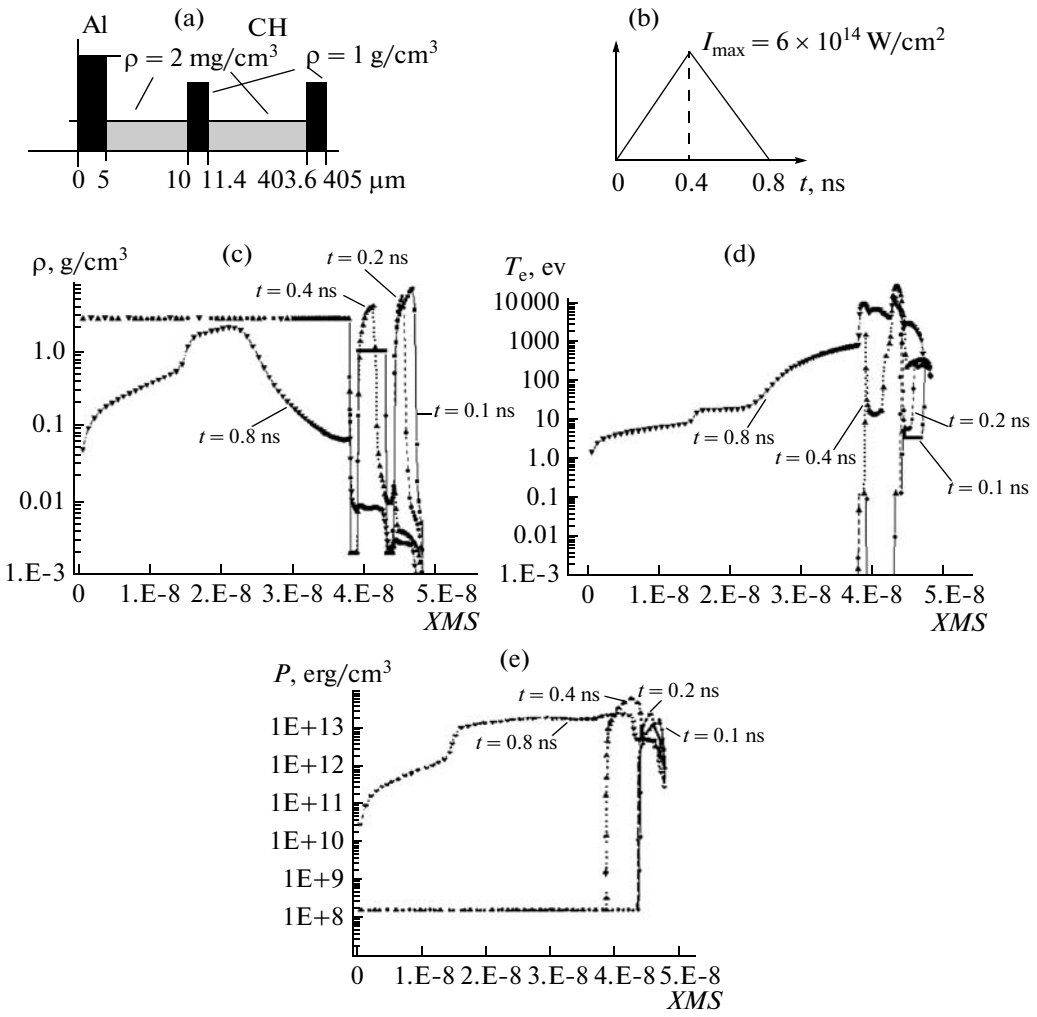

Fig. 3. (a) Density distribution along the 0*Z* axis, (b) temporal form of a laser pulse, dependences of (c) density and (d) electron temperature on the mass coordinated along the 0*Z* axis at the noted time points, and (e) density vs. mass coordinate at the time points $t = 0.1$, 0.2, 0.4, and 0.8 ns. By the time $t = 0.8$ ns, discharging has passed and the left (back) part is being scattered along the direction of laser beam.

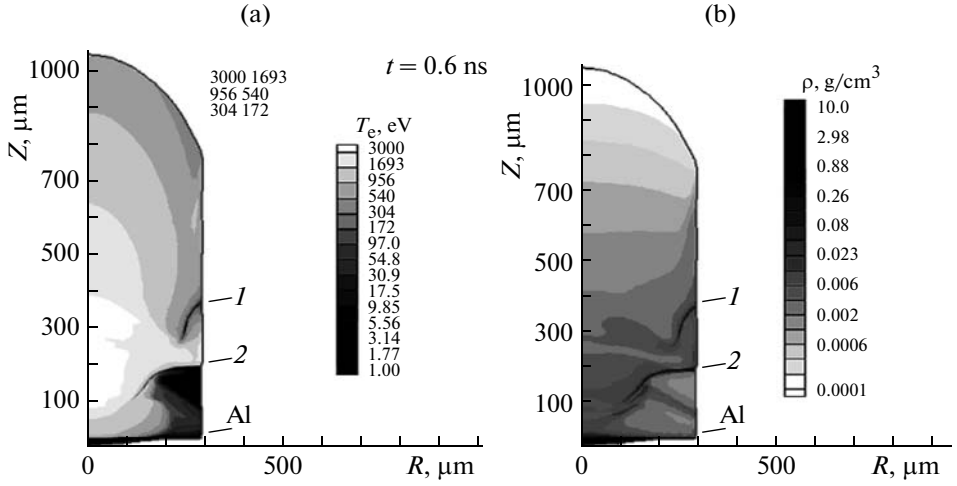

Fig. 4. Two dimensional (a) temperature and (b) density fields at the time instant $t = 0.6$ ns: positions of (*1*) the first and (*2*) the second CH layers.

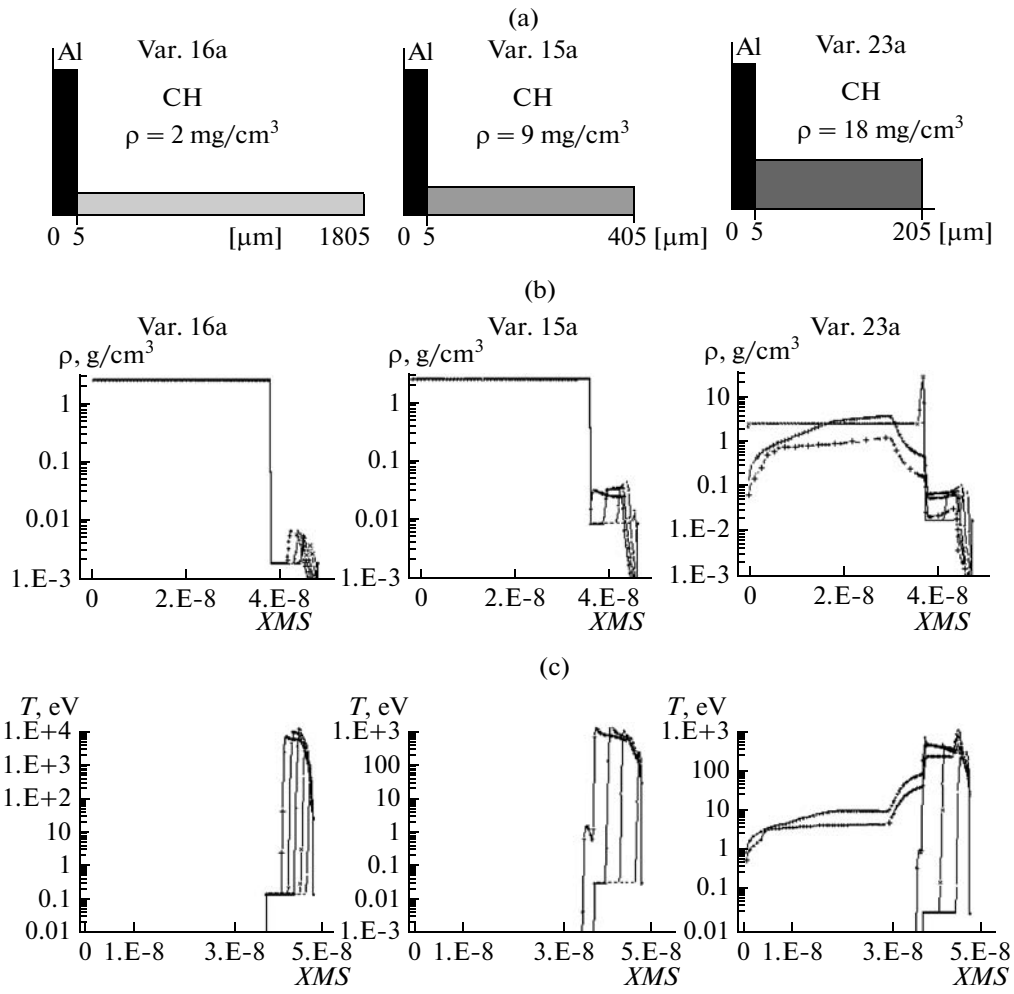

Fig. 5. (a) Setting of the problems (variants 16a, 15a, and 23a). The bulk mass of the target is the same in all three cases, but the initial densities are different. (b) Density and (c) temperature vs. mass coordinate *XMS* at the time points 0.2, 0.4, 0.6, and 0.8 ns for variants 16a, 15a, and 23a.

Computations of the following variants have been performed: (1) variant 16a: the density of the external layer $\rho_0 = 2$ mg/cm^3 and thickness of 1800 μm; (2) variant 15a: $\rho_0 = 9$ mg/cm^3 and a thickness of 400 μm; and (3) variant 23a: $\rho_0 = 18$ mg/cm^3 and a thickness of 200 μm. In all three computations, the bulk mass of low-density matter was the same. Figure 5a represents the setting of the problem.

Figures 5c and 5c represent the results of computations. In these computations, the assumption that the velocity of propagation of the hydrothermal wave depends only on the bulk mass was tested. This assumption proved to be wrong.

In the next series of one-dimensional and two-dimensional computations, the thickness of porous matter was the same and equal to 400 μm and the initial density varied. Figure 6a represents the setting of the problem: (1) variant 25a, when the initial density of the external layer was 4.5 mg/cm^3; (2) variant 15a, when the initial density was 9 mg/cm^3; and (3) variant 24a, when the initial density was 18 mg/cm^3.

In all three cases, the thickness of the external layer was 400 μm. Figures 6b–6d show the temperature and density vs. coordinate z at different time points. In the variant with the initial density of 4.5 mg/cm^3, the wave reached the surface of the aluminum layer by the time of 0.6 ns; in the variant with the initial density of 9 mg/cm^3, by the time of 0.8 ns; and, in the case with the initial density of 18 mg/cm^3, the wave had not reached this surface by the end of the pulse. The average velocity of propagation of the hydrothermal wave in these variants was (1) $\bar{V} = 690$ km/s, (2) $\bar{V} = 526$ km/s, and (3) $\bar{V} = 375$ km/s. In the computation

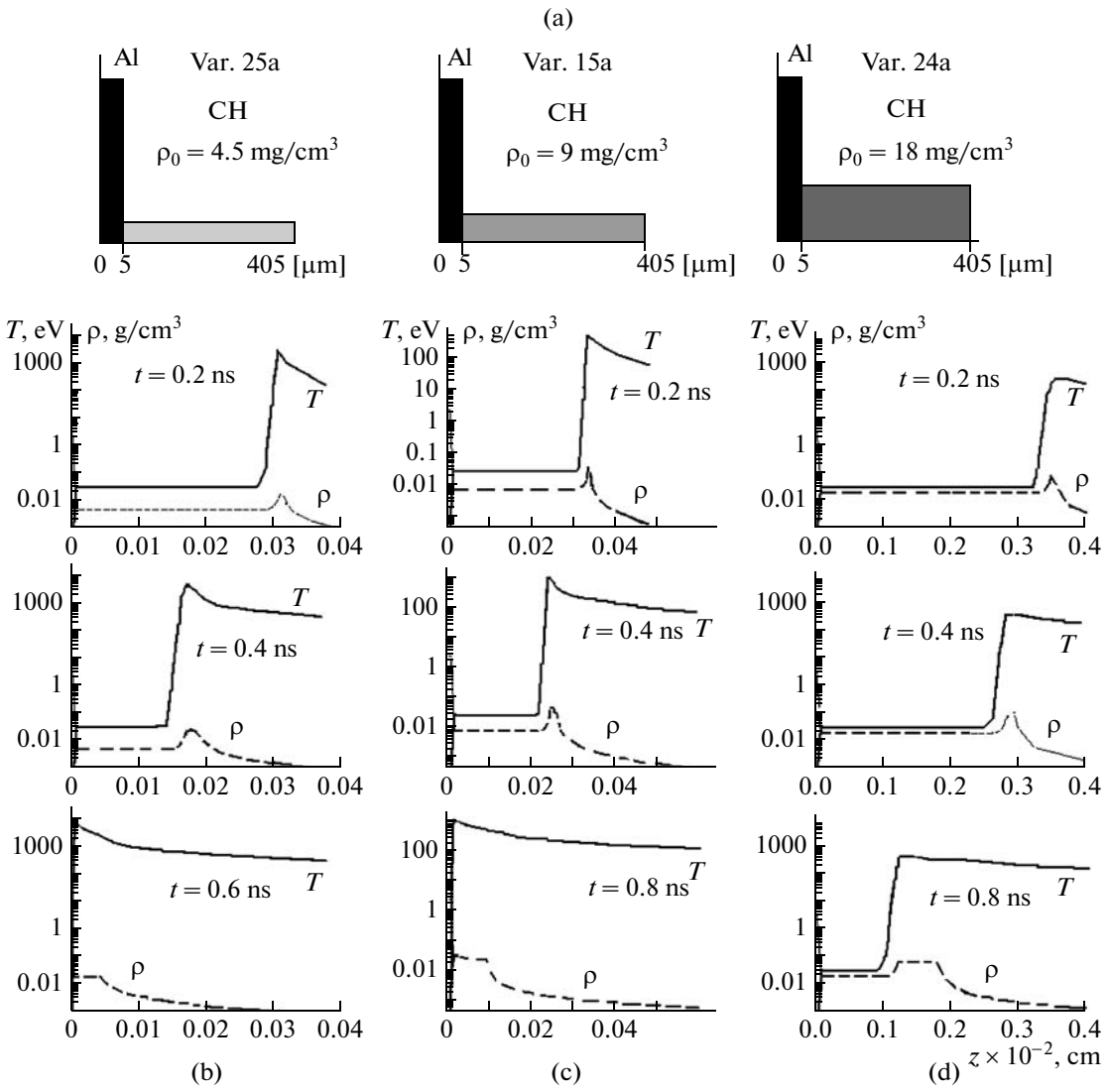

Fig. 6. (a) Setting of the problems for three variants with different initial densities and the same thicknesses of layers and dependences of density and temperature on Z at different time points for the initial densities of (b) 4.5, (c) 9, and (d) 18 mg/cm^3.

with the initial density $\rho_0 = 2.25$ mg/cm^3, the average velocity was $\bar{V} = 814$ km/s. In that case, the laser radiation passed through a low-density layer significantly earlier that the pulse terminated.

The electron temperature in the plasma significantly exceeded the ion temperature.

The wave velocities obtained in our one-dimensional experiments are somewhat greater than those obtained in the experiments. It should be noted that the diameter of the radiation focusing spot was 300 μm and the layer thickness was 400 μm. This geometric factor had to affect the velocity of wave propagation. A two-dimensional computation of the following variant was performed: the initial density was $\rho_0 =$ 9 mg/cm^3 and the thickness of the external layer was 400 μm. The dependence of the radiation intensity on the radius had the Gaussian form $I_{\max} \sim \exp(-(r/R_f)^2)$ with $R_f = 150$ μm. The transverse radius of the computational domain was $R_0 = 600$ μm. Figure 7 shows the density and temperature distributions along the $0Z$ axis at different time points (0.2, 0.4, and 0.8 ns). By the time $t = 0.8$ ns, the hydrothermal wave is approximately at a distance of 100 μm from the aluminum layer. In two-dimensional computations, the velocity of propagation of this wave was noticeably smaller and agreed with the experimental data.

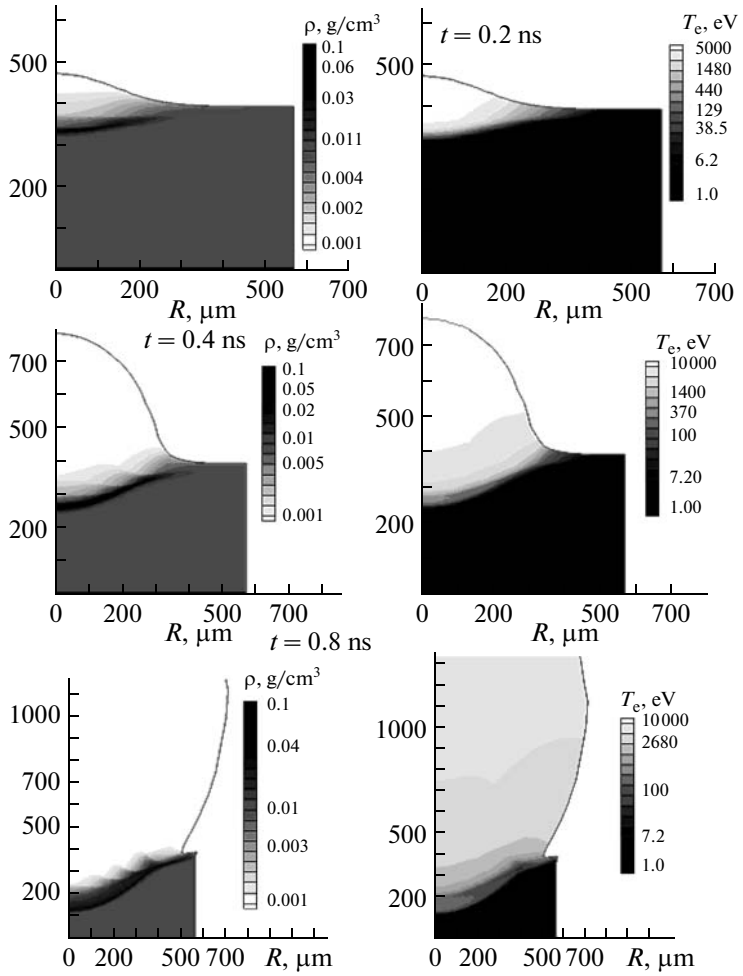

Fig. 7. Density and temperature fields at the time points $t_1 = 0.2$ ns, $t_2 = 0.4$ ns, and $t_3 = 0.8$ ns in variant 15a_2D ($\rho_0 = 9$ mg/cm^3).

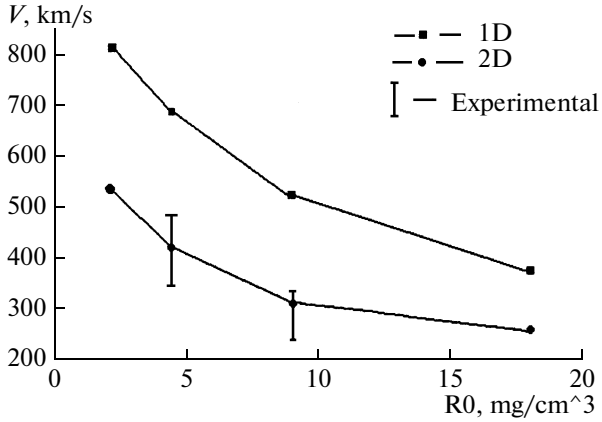

Fig. 8. The velocity of propagation of hydrothermal wave vs. initial density of a low-density medium ρ_0 in one dimensional (1D) and two-dimensional (2D) cases. Vertical "I" shows experimental data.

Thus, in order to attain the agreement between the calculated and experimental data, one has to formulate a model taking into account a substantial decrease in the depth of penetration of laser radiation and heat transfer in such a medium.

In our opinion, after evaporation of the walls of the pores, the plasma remains turbulent for rather a long time. We suggest replacing the quantity ν_e in the formulas for plasma transfer coefficients by the effective collision frequency, which can be significantly greater that the collision frequency in a laminar plasma.

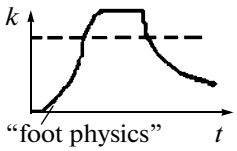

Fig. 9. Schematic description of the time dependence of laser radiation absorption coefficient k.

The electronic thermal conductivity coefficient can be expressed via this frequency. It equals $\kappa_e = \nu_e V_e l_e = n_e V_e^2/\nu_{ef}$, where n_e and V_e are the electron concentration and velocity and l_e is the electron free path. The frequency of energy exchange between the electron and ion components can be determined from the expression $\nu_{ei} = \dfrac{m_i}{m_e}\max\{\nu_e, \nu_{ef}\}$. If $\nu_{ef} \gg \nu_e$, the electronic thermal conductivity in a hot plasma will be automatically suppressed, and the electron and ion temperatures are approximately equal.

The effective collision frequency can be written as $\nu_{ef} = c/l_p$, where the l_p is a parameter having the dimension of length. By analogy with the model of turbulent mixing suggested in [37], it can be interpreted as a certain size of turbulent pulsations, characterizing the energy transfer in such an inhomogeneous plasma. It must be determined a priori. Substituting it in (2), we obtain

$$k_{ab}(\rho) = \frac{\rho(r, z, t)}{\rho_{cr} l_p \sqrt{1 - (\rho/\rho_{cr})}}. \tag{4}$$

It should also be noted that the velocity of wave propagation in a rough grid depends on the cell size. Computations with various numbers of cells in a low-density medium were made, and it was shown that, in order that the propagation velocity depend on the number on cells weakly, it is necessary that the cell size be less than l_p.

Figure 8 shows the dependences of the average velocities of the hydrothermal wave for different values of the initial density ρ_0 in one-dimensional and two-dimensional cases. It is readily seen that our model makes a satisfactory description of wave propagation in a low-density region. Parameter l_p is specified from the condition of matching with the data of measuring the velocity of the hydrothermal wave (it is in the range of l_p from 0.5 to 5 μm).

A question arises if there is a possibility to determine this parameter from other, independent measurements. In the experiments with the PALS installation, the fraction of laser energy that passed through the layer of porous matter of the depth d (in the absence of an aluminum substrate) was also measured. One can introduce the conception of integral radiation absorption depth L_p for the entire time of action of a laser pulse and define it by a simple formula $L_p = -d/\ln(q_{out}/q_{in})$. Here, q_{out} and q_{in} are the intensities of radiation passed through the layer and incident, respectively. We also may assume that there is a direct functional dependence between L_p and l_p. However, this dependence has rather a sophisticated form. Figure 9 shows a schematic dependence of the absorption coefficient in a porous medium, k, on the time t. It should be noted that $L_p \sim 1/k$. At the initial stage, the plasma is absent and the porous medium is transparent for radiation. Along with the heating, plasma, which absorbs radiation (the radiation absorption coefficient in this case increases), is produced. In the American terminology, the initial stage of formation of strongly nonequilibrium plasma is termed the "foot physics" and not described yet by our model. During the heating of the porous medium, the thickness and density of the layer vary. After the hydrothermal wave emerges on the back side of the layer, the radiation absorption coefficient sharply decreases (Fig. 9). A thorough comparison of computational and experimental data is necessary for establishing the dependence of L_p on the parameters of radiation and target, which will enable one to find the functional dependence $l_p = f(L_p)$.

In the experiments [38, 39], a weak optical luminescence was observed at the initial stage of irradiation of the target and, then, approximately 1–4.5 ns after termination of the pulse at the back side of the target. Apparently, this effect is caused by penetration of laser radiation through a low-density structured medium before homogenization of this medium takes place. This radiation leads to the evaporation of the external aluminum layers.

A series of one-dimensional computations with the initial density of the medium $\rho_0 = 4.5$ and 9 mg/cm^3 and $l_p = 0.5$–5 μm was made. The laser pulse energy was 170 J ($I_{max} = 6 \times 10^{14}$ W/cm^2), and

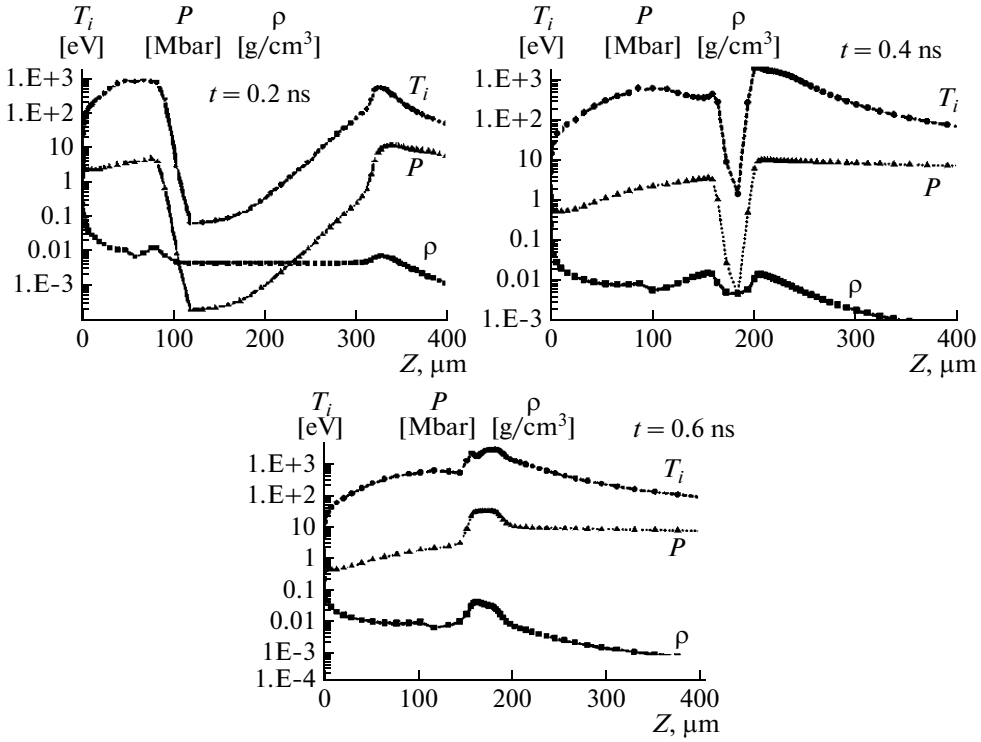

Fig. 10. Distributions of temperature T_i, pressure P, and density ρ at the time points t = (a) 0.2, (b) 0.4, and (c) 0.6 ns. Collision of fluxes took place in the time interval of 0.4–0.5 ns.

the radiation wavelength was 0.438 μm. It was assumed in the computations that, in the time interval $0 < t < 0.1$ ns, the absorption coefficient in a low-density medium was $k(\rho) = 0$ and, then, varied according to (4). In this variant, approximately 3% of the laser energy at the initial stage passes through the porous medium and evaporates the external aluminum layers. As a result, two shock waves are produced: one of them moves into the depth of the aluminum substrate and the other moves in the low-density medium against the laser beam. The first wave reaches the back surface of the aluminum layer by the time of 0.155 ns, and the discharging takes place, i.e., the aluminum layer bestirs. It should be noted that, in the experiments, the weak luminescence in the optical band appeared from the back side of the target, starting from the time instant ~0.2 ns. Computations of propagation of the shock wave in the aluminum layer with a thickness of 5 μm were performed using a more sophisticated QEOS model of the equation of state. In that case, the shock wave came to the back side of the aluminum layer by the time of 0.175 ns and the temperature of compresses matter was about 8 eV.

Starting from the time instant $t = 0.1$ ns, the external layers of the low-density target absorb the radiation and the hydrothermal wave is formed, which moves in the direction of the incident laser beam. Two waves in a low-density medium move against one another and collide by the time $t \geq 0.5$ ns. The collision of hot plasma fluxes forms a temperature of 2–3 keV in plasma and leads to an increase in the brightness of radiation in the X-ray band (which was observed in the experiments by the time $t \geq 0.6$ ns).

Below, the results of one-dimensional computation for the case of the initial density of 4.5 mg/cm^3 are presented. After the collision, the shock moves towards the aluminum substrate (see Fig. 10). Figure 10 shows the distributions of density ρ, pressure P, and ion temperature T_i in the region $0 < Z < 400$ μm.

By the time of pulse termination, the perturbation reaches the dense aluminum layers (due to the discharging, the density is smaller than the initial one, 2.7 g/cm^3, and aluminum flies mainly with a velocity of 10–50 km/s in the direction opposite to that of the $0Z$ axis).

Figure 11 shows the distributions of gas-dynamic parameters vs. the mass coordinate: Figs. 11a–11c, for propagation of the first shock wave over aluminum; Figs. 11d–11f, for propagation of the shock wave formed by the hydrothermal wave.

Figure 12 shows the velocity distribution along the $0Z$ axis in aluminum at the time points $t = 0.8$, 1.2, and 1.5 ns. It is readily seen from Fig. 12, that by the time $t = 0.8$ ns, the left edge of aluminum flies in the

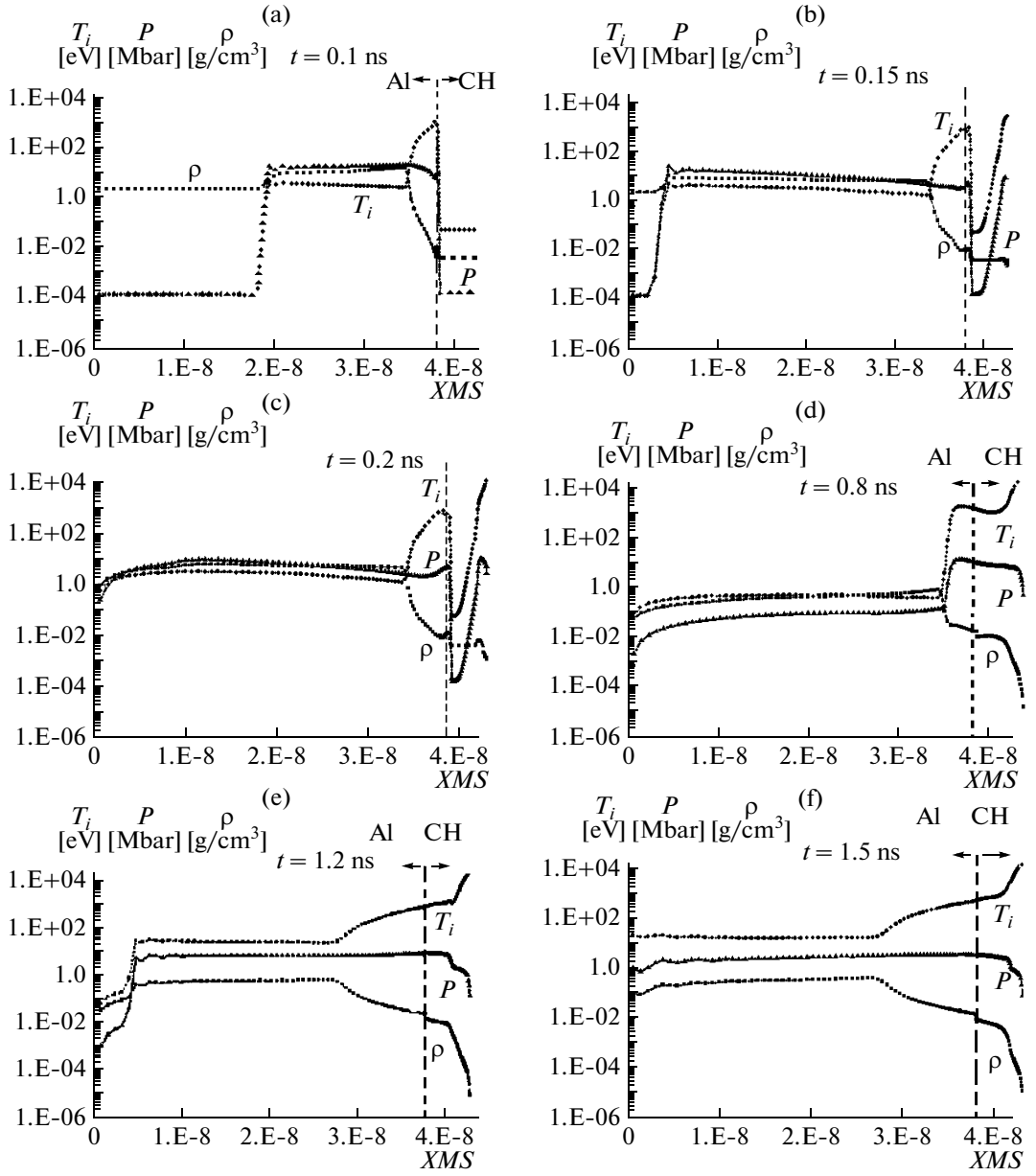

Fig. 11. The temperature and density vs. mass coordinate at the time points (a) 0.1, (b) 0.15, (c) 0.2, (d) 0.8, (e) 1.2, and (f) 1.5 ns. The vertical dashed line corresponds to the aluminum–polymer interface.

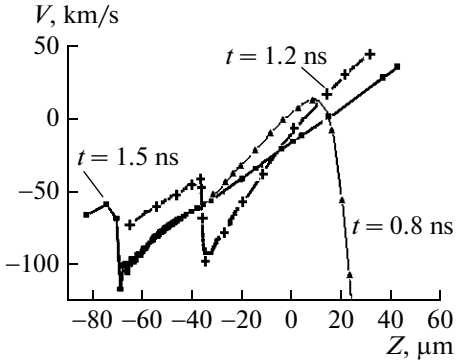

Fig. 12. Velocity of aluminum distributed along $0Z$ axis at the time points $t = 0.8$, 1.2, and 1.5 ns.

negative direction with a velocity of 50 km/s and the central part is practically immobile. The front evaporated layers have been captured by the hydrothermal wave and move at a high speed in the negative direction. After colliding with the dense target ($t = 1–1.2$ ns), a part of the aluminum plasma acquired positive direction and the remaining part flew to the negative direction with a high speed. Finally, as seen from Fig. 11, by the time $t = 1.5$ ns, the pressure in aluminum (in the main part) has been leveled and the matter flies in the negative direction; moreover, the edge moves with a velocity of 70 km/s, i.e., the main mass overtakes it. At subsequent time instants, the edge layers accelerate to 100 km/s.

As seen from the computations, by the time instant $t \approx 1.5–1.6$ ns, the perturbation (the jump in temperature and pressure) comes to the back side of the metal layer. This effect can explain the luminescence in the optical band observed experimentally from the back side of the aluminum substrate after termination of a laser pulse for rather a long time (as long as 2 ns). Moreover, the maximum intensity of this luminescence is observed with a delay of 0.7–1.4 ns with respect to the laser pulse.

CONCLUSIONS

A simplified physico-mathematical model presuming the existence of a homogeneous (nonstructured) matter with a density complying with the density of a polymer aerogel has been suggested. It is assumed that the absorption of laser radiation and transfer coefficients depend on the turbulent frequency or the size of turbulent pulsations l_p. This size must be determined a priori from the condition of matching with the experimental data. This model makes possible a satisfactory description of the motion of hydrothermal wave and heat transfer along with some peculiarities of the observed luminescence of plasma.

The new model has been complemented by the condition of passage of laser radiation at the initial time instant, which enabled us to simulate the experimentally observed counter motion of the plasma from a polymer aerogel and the plasma from aluminum foil. It has been shown that the counter motion of Al-plasma leads to a collision with the hydrothermal wave and an increase in the plasma temperature. (It should be noted that the inhomogeneity of the plasma flow and an increase in the brightness of the X-radiation at the time of ≥0.6 ns have been observed in [25, 38].) The passage of the first shock wave through the aluminum substrate enables one to explain the origination of a weak luminescence in the optical band by the time of ≥0.2 ns. The emergence of the pressure pulse from the thermal wave on the back side of the aluminum substrate by the time ~1.5–1.6 ns explains the observed sharp increase in the luminosity in the optical band with a delay of the order of 1 ns from the maximum of the laser pulse intensity.

In the subsequent works, we suppose a further development of our physico-mathematical model. In particular, on the basis of the comparison of the real and numerical experiments, we are going to elaborate methods for determining the value of l_p depending on the structure, initial density of medium, and intensity of the laser radiation.

When this article had already been sent to print, work [40] was issued. In this work, the results of experiments with the PALS installation were also analyzed. In particular, the computations were made there under assumption that the laser energy absorbed by the plasma was only 10–15% of the incident energy. In our opinion, this assumption disagrees with the results of works [35] and [8]. In the latter one, it was suggested to use low-density porous coatings in order to increase the absorption of laser energy in the target. Of course, the final word rests in a well arranged and conducted experiment on measuring the laser energy reflected from a target in the PALS installation. Therefore, one of the conclusions from this work is the suggestion to conduct such experiments in it.

We would also like to recall that, in our joint works with our Czech colleagues, for the first time, from comparison of numerical and real experiments, the symmetrizing effect of a laser prepulse (see [4, 41, 42]) has been demonstrated and recommendations for the use of this approach in laser nuclear fusion have been formulated. The PALS installation gives the possibility to compare—under the same conditions—the efficiency of the first and second methods of symmetrizing the ablation pressure and to elaborate—on the basis of numerical modeling—practical recommendations to improve the symmetry of the compression of nuclear fusion targets in large installations.

ACKNOWLEDGMENTS

We are grateful to N.G. Borisenko and Yu.A. Merkul'ev for placing at our disposal the materials on the PALS experiments and for their useful and critical discussions of our computational results.

REFERENCES

1. N. I. Bokov, A. A. Bunatyan, A. A. Lykov, et al., "The Way to Reduce the Microtarget Sensitivity to Nonsymmetry of Laser Irradiation," PMTF, No. 4, 20 (Novosibirsk, 1982).
2. E. G. Gamaly, A. O. Fedyanin, I. G. Lebo, et al., "Nonlinear Stage in the Development of Hydrodynamic Instability in Laser Targets," Laser and Particle Beams **8,** 399–407 (1990).
3. V. V. Ivanov, A. V. Kutsenko, I. G. Lebo, A. A. Matsveiko, Yu. A. Mikhailov, et al., "Anomalous Burnout of Thing Foils under Heating by Laser Radiation with High Brightness," ZhETF **116,** 1287–1299 (1999).
4. A. B. Iskakov, V. F. Tishkin, I. G. Lebo, J. Limpouch, K. Masek, and K. Rohlena, "Two–Dimencional Model of Thermal Smoothing of Laser Imprint in Double–Pulse Plasma," Phys. Review E **61** (1), 842–847 (2000).
5. J. H. Nuckolls, A. R. Theissen, and G. H. Dahlbacka, US Patent No. 4376752 (15 March 1983).
6. I. G. Lebo, V. F. Rozanov, and V. F. Tishkin, "Hydrodynamic Instability and Target Design," Laser and Particle Beams **12** (3), 361–369 (1994).
7. S. Yu. Gus'kov and V. B. Rozanov, "Interaction between Laser Radiation and Porous Medium and Nonequilibrium Plasma Formation," Kvantovaya elektronika **24** (8), 715–720 (1997).
8. V. B. Rozanov, "On Spherical Compression of the Targets with Thermonuclear Fuel, if Two Laser Beams are Used for Irradiation," UFN **174** (4), 371–382 (2005).
9. M. Dunne, M. Borghesi, A. Ivase, M. Jones, R. Tailor, O. Willi, R. Gibson, S. Oldman, J. Mark, and R. Watt, "Evaluation of Foam Buffer Target Design for Spatially Uniform Ablation of a Laser–Irradiated Target," Phys. Rev. Lett. **75** (21), 3858–3861 (1995).
10. J. Limpoch, N. N. Demchenko, S. Yu. Gus'kov, M. Kalal, A. Kasperczuk, et al., "Laser Interaction with Plastic Foam–Metallic Foil Layered Targets," Plasma Phys. Control. Fusion **46,** 1831–1846 (2004).
11. A. E. Bugrov, I. N. Burdonskii, V. V. Gavrilov, et al., "Interaction between Powerful Laser Radiation and Low–Dense Porous Mediums," ZhETF **111,** 903–918 (1997).
12. T. Afshar-rad, M. Desselberger, M. Dunne, J. Edwards, J. M. Foster, D. Hoarty, M. W. Jones, S. J. Rose, P. A. Rosen, R. Taylor, and O. Willi, "Supersonic Propagation of an Ionization Front in Low Density Foam Targets Driven by Thermal Radiation," Phys. Rev. Lett. **73,** 74–77 (1994).
13. J. A. Koch, K. G. Estebrook, J. D. Bauer, C. A. Back, A. M. Rubenchik, et al., "Time–Resolved X-ray Imaging of High–Power Laser–Irradiated Underdense Silica Aerogels and Agar Foams," Phys. Plasmas **2,** 3820–3831 (1995).
14. A. E. Bugrov, I. N. Burdonskiy, I. K. Fasakhov, V. V. Gavrilov, A. Yu. Goltsov, A. I. Gromov, A. I. Kondrashov, N. G. Kovalskiy, S. F. Medovshchikov, V. G. Nikolaevskiy, V. M. Petryakov, and E. V. Zhuzhukalo, "Laser–Plasma Interaction in Experiments with Low–Density Volume–Structured Media on the "Mishen" Facility," in *Proc. of SPIE*, Ed. by O. N. Krokhin, S. Yu. Guskov, and Yu. A. Merkuliev (Bellingham, WA, 2003), vol. 5228.
15. N. G. Borisenko and Yu. A. Merkul'ev, "The Targets with Microheterogeneous Structure for Spherical Irradiation," in *Works of FIAN* (Nauka, Moscow, 1992), vol. 220, pp. 28–46 [in Russian].
16. J. Falconer, W. Nazarov, and C. J. Horsfield, "In Situ Production of Very Low Density Microporous Polymeric Foams," J. Vac. Sci. Technol. **A13,** 1941 (1995).
17. A. E. Bugrov, I. N. Burdonskii, V. V. Gavrilov, et al., "Processes of Absorption and Dispersion of Powerful Laser Radiation in Low–Dense Porous Mediums," ZhETF **115** (3), 805–818 (1999).
18. N. G. Borisenko, Yu. A. Merkuliev, and A. I. Gromov, "Microheterogeneous Targets – a New Challenge in Technology, Plasma Physics, and Laser Interaction with Matter," J. Moscow Phys. Soc. **4** (3), 247–273 (1994).
19. W. Nazarov, "An In–Situ Polymerization Technique for the Production of Foam–Filled Laser Targets," J. Moscow Phys. Soc. **8,** 251–255 (1998).
20. I. G. Lebo, I. V. Popov, V. B. Rozanov, and V. F. Tishkin, "Numerical Simulation of Thermal Equalizing and Hydrodynamic Compensation in the Targets 'Laser Hotbed'," Kvantovaya elektronika, No. 22, 1257–1261 (1995).
21. A. B. Iskakiv, I. G. Lebo, V. B. Rozanov, and V. F. Tishkin, "On the Neutron Yield in the Two–Beam Scheme of Laser Heating and Compression of Spherical Shell Targets with a Low–Density Coating," Journal of Russian Laser Research **22** (1), 82–89 (2001).
22. S. Yu. Gus'kov, N. N. Demchenko, V. B. Rozanov, et al., "Symmetric Compression of the Targets 'Laser Hotbed' by Little Number of Laser Beams," Kvantovaya elektronika **33,** 95–104 (2003).
23. S. Yu. Gus'kov, N. V. Zmitrenko, I. V. Popov, V. B. Rozanov, and V. F. Tishkin, "2D Energy Transport and Plasma Generation, if the Laser Beam Acts onto the Substance with Subcritical Density," Kvantovaya elektronika **30** (7), 601–605 (2000).
24. S. V. Bondarenko, S. G. Garanin, G. A. Kirillov, Yu. F. Kir'yanov, and G. G. Kochemasov, "Energy Transport in Tridimensional–Structured Medium," Kvantovaya elektronika **31** (1), 39–44 (2001).
25. A. A. Akunets, N. G. Borisenko, D. Klir, V. Kmetik, E. Krousk, I. Limpoukh, K. Masek, Yu. A. Merkul'ev, V. G. Pimenov, M. Pfeier, I. Ulshmid, and A. M. Kholenkov, "Features of Penetration of Laser Radiation with Wave Length of 0.438 μm and Intensity of $(3–7) \times 10^{14}$ W/cm^2 through Subcritical Plasma of Polymeric Aerogels," Preprint No. 8 (FIAN, Moscow, 2007).

26. K. Jungwirth, A. Cejnarova, L. Juha, B. Kralicova, J. Krasa, et al., "The Prague Asterix Laser System," Phys. Plasmas **8,** 2495–3006 (2001).
27. S. I. Braginskii, *Transport Phenomenon in Plasma. Problems of Plasma Theory* (Gosatomoizdat, Moscow, 1963), issue 1 [in Russian].
28. I. G. Lebo and V. F. Tishkin, *Research of Hydrodynamical Instability in the Problems of Laser Thermonuclear Fusion* (Nauka, Fizmatlit, Moscow, 2006), pp. 208–218 [in Russian].
29. Ya. B. Zel'dovich and M. P. Raizer, *Physics of Shock Waves and High–Temperature Hydrodynamic Phenomena. Monograph* (Nauka, Fizmatlit, Moscow, 1966) [in Russian].
30. Yu. V. Afanas'ev, E. G. Gamalii, and V. B. Rozanov, "The Basic Equations of Laser Plasma Dynamics and Kinetics," in *Works of FIAN* (Nauka, Moscow, 1982), vol. 134, No. 10 [in Russian].
31. R. M. More et al., Phys. Fluids **31** (10), 3059 (1988).
32. E. Aristova, A. Iskakov, I. Lebo, and V. Tishkin, "2D-Lagrangian Code LATRANT for Simulation Radiation Gas Dynamic Problems," in *Proc. of SPIE. ECLIM 2002: 27th European Conf. on Laser Interaction with Matter. 7–11 October 2002* (Moscow, 2003), vol. 5228, pp. 131–141.
33. A. B. Iskakov, I. G. Lebo, I. V. Popov, V. B. Rozanov, and V. F. Tishkin, *The Way to Consider Laser Beams Refraction under Simulation of 2D–Heterogeneous Compression of the Targets. Short Reports on Physics* (FIAN, Moscow, 1997), Nos. 1–2, pp. 28–35 [In Russian].
34. I. G. Lebo, N. N. Demchenko, A. B. Iskakov, et al., "Simulation of High–Intensity Laser–Plasma Interactions by Use of 2D Lagrangian Code 'ATLANT–HE'," Laser and Particle Beams, No. 22, 267 (2004).
35. A. I. Lebo, I. G. Lebo, and D. Batani, "The Relationship between the Pressure in Compressed Condensed Substance and Parameters of High–Power Laser Pulses," Kvantovaya elektronika **38** (8), 747–754 (2008).
36. Yu. V. Afanas'ev, E. G. Gamalii, N. N. Demchenko, and V. B. Rozanov, "Laser Radiation Absorption by Spherical Target by Considering the Refraction and Developed Hydrodynamics," in *Works of FIAN* (Nauka, Moscow, 1982), vol. 134, pp. 32–41 [in Russian].
37. S. Z. Belen'kii and E. S. Fradkin, "Theory of Turbulent Mixing," in *Works of FIAN* (Moscow, 1965), vol. 29, p. 207 [in Russian].
38. A. M. Khalenkov, N. G. Borisenko, V. N. Kondrashov, Yu. A. Merkul'ev, J. Limpouch, and V. G. Pimenov, "Experience of Microheterogeneous Target Fabrication to Study Energy Transport in Plasma near Critical Density," Laser and Particle Beams **24** (2) (2005).
39. I. V. Akimova, N. G. Borisenko, A. I. Gromov, A. M. Khalenkov, V. N. Kondrashov, J. Limpouch, E. Krousky, J. Kuba, K. Masek, Yu. A. Merkul'ev, W. Nazarov, V. G. Pimenov, "Regular 3–D Networks for Controlled Energy Transport Studies in Laser Plasma Near Critical Density," Fusion Science and Technology **49** (4), 676–685 (2006).
40. V. Rozanov, D. Brishpoltsev, G. Vergunova, et al., "Energy Transfer in Low–Density Porous Targets Doped by Heavy Elements. The Fifth Intern. Conf. on Inertial Fusion Sciences and Applications (IFSA2007)," Journ. of Physics: Conference Series **112,** 022010 (2008).
41. J. Limpouch, A. B. Iskakov, K. Masek, K. Rohlena, I. G. Lebo, and V. F. Tishkin, "Transverse Structures in Corona of Nonuniformly Irradiated Solid Targets," Laser and Particle Beans, No. 20, 93–99 (2002).
42. Yu. F. Mikhailov, M. A. Grechko, O. A. Zhitkova, M. A. Zhurovich, A. V. Kutsenko, I. G. Lebo, J. Limpouch, A. A. Matsveiko, V. B. Rozanov, G. V. Sklizkov, A. N. Starodub, V. F. Tishkin, and A. M. Chekmarev, "Effect of a Preplus on Ablation–Pressure Smoothing in Laser Heating of Thin Foils," J. of Russian Laser Research **28** (4), 311–325 (2007).